Enhancing antifouling characteristics and performance against protein macromolecule foulant on PVDF membrane ultrafiltration with eco-friendly Arabic gum additive

Radenrara Dewi Artanti Putri, Herlambang Abriyanto, Ria Desiriani, Abdullah Malik Islam Filardli, Zuhriyan Ash Shiddieqy Bahlawan, Maharani Kusumaningrum, Gita Putri Prastiwi, Rica Raihana, Desy Hikmatul Siami & Randi Aswar

Published online: 31 Mar 2023.

Submit your article to this journal

View related articles

View Crossmark data

Taylor & Francis
Taylor & Francis Group

Check for updates

Enhancing antifouling characteristics and performance against protein macromolecule foulant on PVDF membrane ultrafiltration with eco-friendly Arabic gum additive

Radenrara Dewi Artanti Putri[a,b,c] [iD], Herlambang Abriyanto[b,c] [iD], Ria Desiriani[b,c] [iD], Abdullah Malik Islam Filardli[b,c] [iD], Zuhriyan Ash Shiddieqy Bahlawan[a] [iD], Maharani Kusumaningrum[a] [iD], Gita Putri Prastiwi[b,c], Rica Raihana[b,c], Desy Hikmatul Siami[a], and Randi Aswar[a] [iD]

[a]Department of Chemical Engineering, Faculty of Engineering, Universitas Negeri Semarang, Semarang, Indonesia; [b]Department of Chemical Engineering, Faculty of Engineering, Diponegoro University, Semarang, Indonesia; [c]Membrane Research Center (MeR-C), Integrated Laboratory for Research and Services, Diponegoro University, Semarang, Indonesia

ABSTRACT

This study investigated the effects of Arabic gum (AG) on the separation performance of polyvinylidene fluoride (PVDF) membranes. The membrane properties were characterized using scanning electron microscope energy dispersive X-ray (SEM–EDX), Fourier transforms infrared (FTIR), tensile strength tester, and contact angle. Results showed that incorporating AG from 0.5 wt% to 1.5 wt% into PVDF membrane could increase pure water flux from 47.46 L/m^2 h to 66.04 L/m^2 h and porosity from 53% to 58%. Moreover, the highest flux recovery was obtained by PVDF/AG-1.5 membrane, revealing the improvement in fouling resistance against bovine serum albumin (BSA). However, the addition of AG from 0.5 wt% to 1.5 wt% did not affect to increase of membrane mechanical strength and the efficiency of the membranes for BSA rejection. SEM, XRD and FTIR analyses confirmed the successful incorporation of AG, which improved membrane surface hydrophilicity compared to the pristine PVDF membrane. Overall, the obtained result showed that incorporating AG could attain synergy benefits in enhancing the membrane properties and performance.

GRAPHICAL ABSTRACT
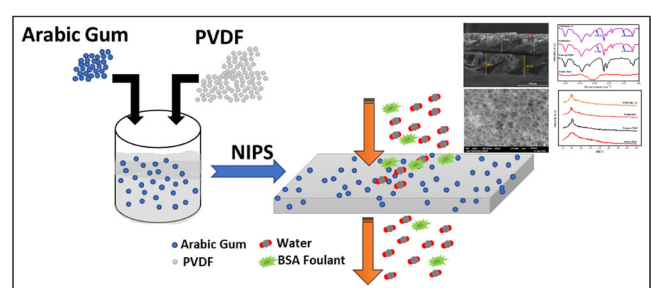
1. Introduction

In the past few decades, membrane separation technology has become essential in water purification and wastewater treatment due to its selectivity and good chemical stability.[1–3] Among various membrane polymers, polyvinylidene fluoride (PVDF) is a commonly used and promising one due to its excellent mechanical strength and high chemical resistance.[4–6] However, the main obstacle to membrane polymer usage is an undesired hydrophobic property that commonly leads to severe membrane fouling.[7] Therefore, the researchers look for some solutions to resolve these issues. Out of many solutions, improving membrane performance through modification of membrane structure via the blending method is promising

technique.[8] A very large number of carbon-based nanoparticles consist of nanotubes,[9] natural inorganic compounds,[10] and the oxides of metals such as iron, silver, and titanium have been exploited to fabricate membrane nanocomposites.[11,12] Incorporating carbon-based nanoparticles into membrane structure could improve hydrophilicity membrane, fouling resistance, an increase mechanical membrane, as explained in many available literature studies.[13] However, there is a big question about the environmental fate of the long-term use of these nanoparticles incorporating membrane polymer. For instance, during membrane filtration, the effluent from membrane filtration directly enters the drain water system, the effluent (permeate) may contain nanoparticles and

---

lead to secondary pollution. Even if the nanoparticles do not pass through the membrane, they could be restrained into the retentate water, resulting in further decay.[14] Nanoparticles in water effluents can be transported to the aquatic systems by rainwater runoff, causing contamination into surface and ground waters. Hence, it is necessary to apply alternative materials with sustainable features for membrane modification.

Natural additives can be used as another preference because they are obtained from natural sources, which provide low toxicity, biocompatible and eco-friendly. Many natural additives are abundantly available for membrane modification. These additives revealed their promising potential to improve membrane performance in water and wastewater treatment. For example, a study observed the fabrication polysulfone membrane incorporating the extracted chlorophyll from spinach and PEG to enhance membrane structure. The result showed that the hydrophilicity, water flux, and humic acid rejection increased significantly compared to the pristine polysulfone membrane.[15] Another study also evaluated the fabrication of an antifouling PVDF membrane with chitosan. They found that the addition of chitosan as a hydrophilic agent result in enhanced hydrophilicity and flux of membrane as well as reduced membrane fouling.[16–18] These natural additives have been utilized directly as raw materials without further modification, but sometimes the modification process is necessary to get good stability of natural additives in membrane structure.

Arabic gum (AG) is a biodegradable, sustainable, and environmentally friendly material that is extracted from some acacia tree species.[19–21] The main content of AG was polysaccharides (∼97%), followed by a few proteins content (∼3%). AG has been recently performed to increase membrane performance in gas separation, desalination, water, and wastewater treatment.[22,23] The high antifouling property of AG is due to the presence of hydroxyl functional groups (–OH). Apart from AG, a natural compound containing many hydroxyl groups is tannic acid. AG and tannic acid are natural compounds used in various industries, including the food, pharmaceutical, and cosmetic sectors. However, their properties and applications are different. AG consumption is generally considered safe and has no known side effects.[24] If consumed in large quantities, tannic acid can adversely affect the human body, including gastrointestinal irritation, liver damage, and kidney damage.[25] In terms of safety and versatility, AG is generally considered superior to tannic acid. AG is a food-grade substance used extensively in the food and beverage industry, whereas tannic acid is used primarily for non-food applications. Hence, adding AG incorporated membrane surface might improve the porosity, pore size, and hydrophilicity of the membrane surface and improve antifouling capabilities while decreasing membrane fouling.

A previous study prepared a polysulfone (PS) membrane blended with different AG contents via the phase inversion technique. The result showed that adding AG to the casting solutions revealed a remarkable enhancement in PS membrane hydrophilicity, flux, and bovine serum albumin (BSA) rejection.[21] AG has also been performed as a pore-forming agent for fabricating waste polyvinyl chloride (PVC). The result demonstrated that the addition of AG not only increases the porosity but also improves hydrophilicity.[22] Interestingly, a study

Table 1. Composition of polymer and AG during the preparation of composite PVDF UF membrane.

Variable	Code	Mass base (100 wt%)	
		PVDF	AG
PVDF 13 wt%	PVDF	13.00	–
PVDF 13 wt%/AG 0.5 wt%	PVDF/AG-0.5	13.00	0.50
PVDF 13 wt%/AG 1.0 wt%	PVDF/AG-1.0	13.00	1.00
PVDF 13 wt%/AG 1.5 wt%	PVDF/AG-1.5	13.00	1.50

reported that incorporating AG into a membrane polymer solution may increase the mechanical property of the membrane. This enhancement of mechanical behavior in the membrane could be due to the addition of AG creating a plasticizing effect, resulting in improved mechanical strength.[23]

Thus far, the addition of AG has not been used as an additive in PVDF membrane fabrication. Hence, the novelty of this study was AG usage as an additive for the first time embed into a PVDF membrane polymer solution. This study aimed to evaluate the effect of different AG concentrations on the performance of PVDF membranes by observing some important parameters such as hydrophilicity, morphological membrane structure, chemical membrane surface, flux, porosity, pore size, and mechanical strength.

2. Experimental

2.1. Materials

Polyvinylidene fluoride (PVDF), a membrane polymer substance, was acquired from Kynar (China). *N,N*-Dimethylacetamide (DMAc) from Merck (Germany) served as the organic solvent. In addition, Arabic gum (AG) from Sigma-Aldrich (Germany) was used. As an organic foulant, bovine serum albumin (BSA) was purchased from Agdia, Inc. (Elkhart, USA). Demineralized water is used as a nonsolvent compound obtained from our laboratory.

2.2. Methods

2.2.1. Preparation of PVDF/AG membranes

The AG additive compound was put into the DMAc solution and stirred for 2 h for even dispersion. PVDF is progressively added with an amount of 13% wt. Because the addition of PVDF makes the dope solution dense, it must be introduced gradually and helped by a temperature of 70 °C to reduce the viscosity of this solution. The mixture was left overnight to entirely deflate the air bubbles at room temperature after being agitated for 24 h to create a homogenous solution. The membrane was made by pouring a dope solution onto a 300 μm thick glass plate while maintaining ambient temperatures of 26–30 °C and relative humidity levels of 60–75%. The newly produced membrane was immediately submerged for 24 h in 1 L of demineralized water. The membrane was then taken off, and dried for 24 h at 60 °C to remove any remaining water and solvent. The membrane is trimmed to fit the cross-flow tester's size. The composition of membrane dope solutions with variations in the addition of AG is shown in Table 1.

2.3. Characterization

2.3.1. Pure water flux (PWF), overall porosity and pore size

The Amicon 8010 (Millipore) cell model was used in a dead-end stirred filter system to conduct the pure water flux test. To prevent compaction effects, each membrane was compressed prior to flow measurement by filtering clean water at 4 bar for at least an hour. Equation (1) is used to calculate the flux.

$$J_{pwf} = \frac{V}{A \ x \ t} \tag{1}$$

where J_{pwf} is the PWF of the membrane in L/m^2 h1 and V is the volume of permeate collected over time (h) with an area of A (m^2).

Determination of membrane porosity using dry-wet gravimetric method. Membrane sheets of a certain size were soaked for 24 h in distilled water before being cleaned with tissue paper. To determine the dry weight of the membrane, the membrane was weighed, dried at 70 °C, and reweighed. Three repetitions were done this way until the dry membrane weight stayed the same. The membrane porosity is calculated using Equation (2).

$$\varepsilon = \frac{w_w - w_d}{\rho_w \ \times \ \delta \ \times \ A} \ \times \ 100\% \tag{2}$$

where ε is the membrane porosity, ρ_w (997 kg/m^{-3}) is the weight of water per cubic meter, W_w and W_d are the weights of the wet and dry membranes, respectively, A is the effective membrane area (m^2), and δ is the membrane thickness (m). The mean pore size was determined using the filtering rate method and the Guerout–Elford–Ferry calculation. Equality (3) can be applied to the following formula to determine the pore size (r_m):

$$r_m = \sqrt{\frac{(2.9 - 1.75 \ \varepsilon) \ \times \ 8\eta\delta Q}{\varepsilon \ \times \ A \ \times \ \Delta P}} \tag{3}$$

where δ is the membrane thickness (m), Q is the volume of permeate per unit time (m^3/s), and P (Pa) is the trans-membrane pressure. Where η is the viscosity of pure water (8.9×10^{-4} Pa s).

2.3.2. Fourier transform infrared (FTIR) and X-ray diffraction (XRD) analysis

Membrane functional groups were studied by using Fourier transform infrared spectroscopy (Perkin Elmer/Spotlight 400 Frontier spectrometer/USA). The FTIR spectra of the membrane samples were acquired in the 400–4000 cm^{-1} wavenumber range. X-ray diffraction (XRD; Shimadzu, Japan) was used to determine phase identification and unit cell size. The spectrum was captured using a glass slide monochromator filter waveform at 30 kV and 30 mA with a scanning speed of 4 degrees/min.

2.3.3. Scanning electron microscope (SEM) analysis

The surface morphology images of all additives and membranes were scanned using a scanning electron microscope (Phenom Pro X desktop SEM with EDX, The Netherlands). Cross-sectional morphology was seen at a 10,000x magnification, whereas surface morphology was at 2,000× and 10,000×. Energy dispersive X-ray (EDX) analysis was used to analyze the chemical composition of the samples of natural additives for AG and the produced membranes, including their elemental content.

2.3.4. Contact angle

Contact angle is used to evaluate the hydrophilicity of the membrane surface. Using the OCA 25 from Data Physics Instrument GmbH in Germany, fall contact angles for both static and dynamic falls were measured. The syringe injects five microliters of water onto the membrane's surface. The static contact angle was measured by dripping distilled water on the surface of the membrane. In the first second of dripping, the direct contact angle is calculated. This is done to determine the direct interaction of the membrane surface with distilled water. The dynamic contact angle is measured similarly to the static contact angle. Still, the angle value is measured once every 1 min for 10 min to determine the absorption of water that enters the membrane pores through the membrane surface. The membrane contact angle was calculated at five randomly chosen drop sites on the membrane surface to ensure high measurement accuracy.

2.4. Performance test

2.4.1. Adsorptive fouling

Samples of membrane were compressed for at least an hour. At a pressure of 4 bar, the flux of clean water was then measured. The membrane surface was then exposed for 3 h without flux while being stirred at 250 rpm in empty cells that had previously been filled with BSA solution (1 g/L). The membrane surface was then washed once the BSA solution had been discarded. Then, the flux adsorption was determined. Utilizing the flux recovery (FR) and equation, we demonstrate how to evaluate the propensity to absorb fouling (4).

$$\%FR = \left(1 - \frac{J_O - J_a}{J_O}\right) \ \times \ 100\% \tag{4}$$

where % FR is flux recovery (%), J_o is membrane flux before contact with BSA (L/m^2 h) and J_a is membrane flux after contact with BSA (L/m^2 h)

2.4.2. Ultrafiltration cross-flow

Pure water was filtered through membrane samples at a pressure of 4 bar for 30 min, after which the pressure was gradually reduced to 3 bar. BSA solution (1 g/L) was added to the pure water after the pressure had settled and the flux (J) had been measured. The recycling volume is considerably more significant than the volume sampled for analysis to maintain a steady feed concentration. In addition, the feed tank receives the retentate and permeate. Every experiment was run at constant transmembrane pressure and room temperature.
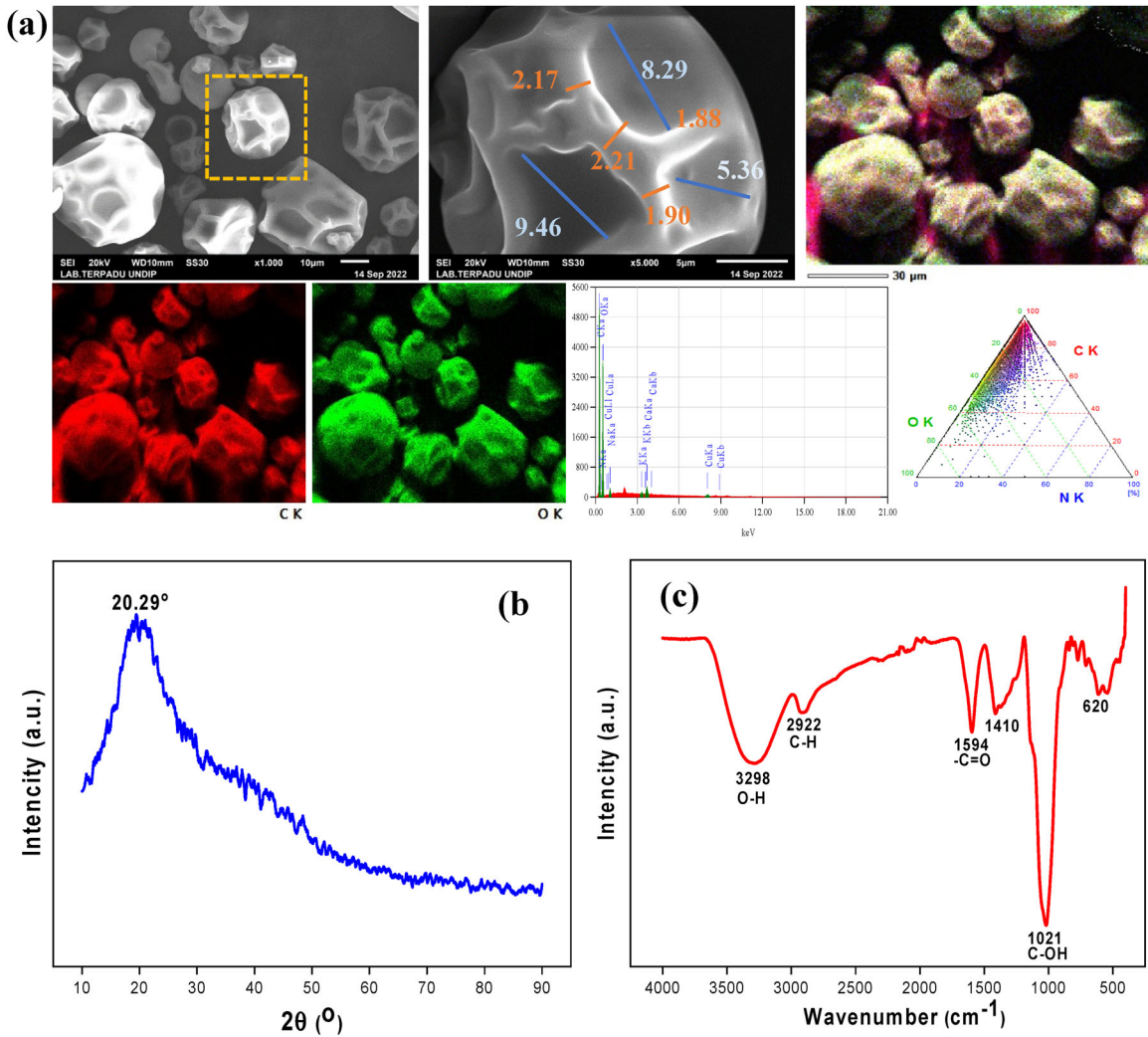
Figure 1. Characterization result of GA: (a) SEM and elemental mapping image and EDX spectra, (b) XRD diffractograms and (c) FTIR spectra.

2.4.3. Analysis of fouling resistance

In this research, we identified reversible fouling (F_r), irreversible fouling (Fi_r), and the total fouling ratio (F_t). Equations (5)–(7) were used to calculate the values of F_r, Fi_r, and F_t, respectively:

$$F_r = \left(\frac{J_a - J}{J_o}\right) \times 100\% \quad (5)$$

$$F_{ir} = \left(\frac{J_o - J_a}{J_o}\right) \times 100\% \quad (6)$$

$$F_t = \left(1 - \frac{J}{J_o}\right) \times 100\% \quad (7)$$

Furthermore, there are various factors for membrane fouling, such as membrane resistance, cake layer resistance, and fouling resistance. In principle, to evaluate the degree of membrane fouling, the filtration resistance will be calculated by Darcy equation in Equations (8)–(11) [3]:

$$R_m = \frac{\Delta P}{\mu \times J_O} \quad (8)$$

$$R_m + R_f = \frac{\Delta P}{\mu \times J_a} \quad (9)$$

$$R_c = R_t - (R_m + R_f) \quad (10)$$

$$R_t = R_m + R_c + R_f = \frac{\Delta P}{\mu \times J} \quad (11)$$

where R_t, R_m, R_f, and R_c (m^{-1}) demonstrates the total filtration resistance, membrane resistance, fouling resistance, and cake layer resistance of membranes, respectively. ΔP was transmembrane pressure (3×10^5 Pa), and μ was water viscosity (8.9×10^{-4} Pa s). J_o, J, and J_a were water permeate, permeate flux of BSA, and permeate flux of BSA after cleaning, respectively.

2.4.4. Analysis of membrane stability

The stability test was conducted in the same manner as our earlier paper.[12] This stability test aimed to ascertain how long the membrane would last in the water. The membrane was shaken for 14 days in a closed Erlenmeyer tube filled with distilled water at 28 °C and 100 rpm. After 14 days, the membrane was dried in oven at 60 °C for 24 h to remove the water content in the membrane pores. The remaining

Arabic gum group content in the membrane was then evaluated using FTIR. A cross-flow test including multiple BSA filtering cycles and washing with distilled water, was used to test the membrane's recycle resistance performance.

3. Results and discussions

3.1. Additives characterization

The natural additive AG was also characterized using PSA, FTIR, XRD, and SEM-EDX. The SEM analysis was performed to study the morphology of AG, and the results are shown in Figure 1a. Figure 1a presents the SEM images of AG was a spherical shape with some cavity around the particle surface. Arabic gum is a complex composite of glycoproteins, polysaccharides, and salts with a matt surface texture and a pale white to orange-brown color range. It takes on a paler, glassy appearance when crushed, resulting in solid spherical shreds of varying sizes. This splitting and crushing process causes a cavity on the Arabic gum's surface. These cavity cause AG size become shrink and become smaller. The cavity size of one particle in AG has a diameter average of $7.52 \pm 2.24 \, \mu m$. The Arabic gum's diameter, measured manually with ImageJ software, was $53.26 \pm 3.64 \, \mu m$. This result was also confirmed by laser particle size analyzer (LPSA) result, which showed that the AG belongs to microparticle groups with an average diameter of AG was $58.826 \, \mu m$.

The elements distribution of AG was characterized by EDX, as listed in Table. 2. The primary elements in AG consist of O (47.84%mass) and C (50.28%mass). Meanwhile, the AG also contains some mineral elements such as Ca (0.52%mass), Na (0.52%mass), and K (0.14%mass). A similar result was also seen in other available literature studies. The major mono-saccharides in AG include L-arabinose, L-rhamnose, D-glucuronic acid, 1,3-linked-D-galactopyranosyl bonds, and a few mineral salts (K and Ca).[19,26]

The XRD patterns of AG were demonstrated in Figure 1d. The diffraction peaks at $2\theta = 20.29°$ indicated that the AG has an amorphous crystalline structure with a random arrangement in AG particles.[27] FTIR spectra of AG were demonstrated in Figure 1e. The characteristic peaks of AG at wavelength $3000–3500 \, cm^{-1}$ (peak at $3298 \, cm^{-1}$) confirmed –OH groups in AG structure,[28,29] leading to improve hydrophilicity property of PVDF/AG membrane. The band around wavelength $2922 \, cm^{-1}$ indicated the stretching of C–H groups.[30] The peaks at wavelength $1021 \, cm^{-1}$ and $600 \, cm^{-1}$ were attributed to C–OH in polysaccharides molecules and the stretching of pyranose ring in polysaccharides.[31] The spectrum of Arabic gum shows a characteristic peak at $1594 \, cm^{-1}$ due to the $–C=O$ stretching vibration of the carboxylate group.[27] The results of the data from FTIR, which aim to determine the organic bonds between groups that exist in this Arabic gum, correspond with the results shown by the EDX analysis, which shows the amount of elemental content present.

3.2. Water flux, porosity, and pore size of membrane

The characteristics of UF membranes, such as the porosity and pore size of the membrane, later influence the flux value of a membrane and significantly impact performance in the filtration process. Figure 2 displays the PVDF/AG membrane's pore size distribution, porosity, and flux values. Figure 2a presents the properties of PVDF and PVDF/AG membranes at different AG concentrations toward pure water flux and porosity. Compared to the pristine PVDF membrane, the pure water flux increased from $47.46 \, L \, m^{-2} \, h^{-1}$ for pristine PVDF membrane to $65.79 \, L \, m^{-2} \, h^{-1}$; $64.92 \, L \, m^{-2} \, h^{-1}$ and $66.04 \, L \, m^{-2} \, h^{-1}$ for PVDF/AG-0.5, PVDF/AG-1, and PVDF/AG-1.5 after 60 min of filtration, respectively. According to numerous studies, a membrane with a higher porosity forms more pores on its surface, permitting more water to enter the permeate
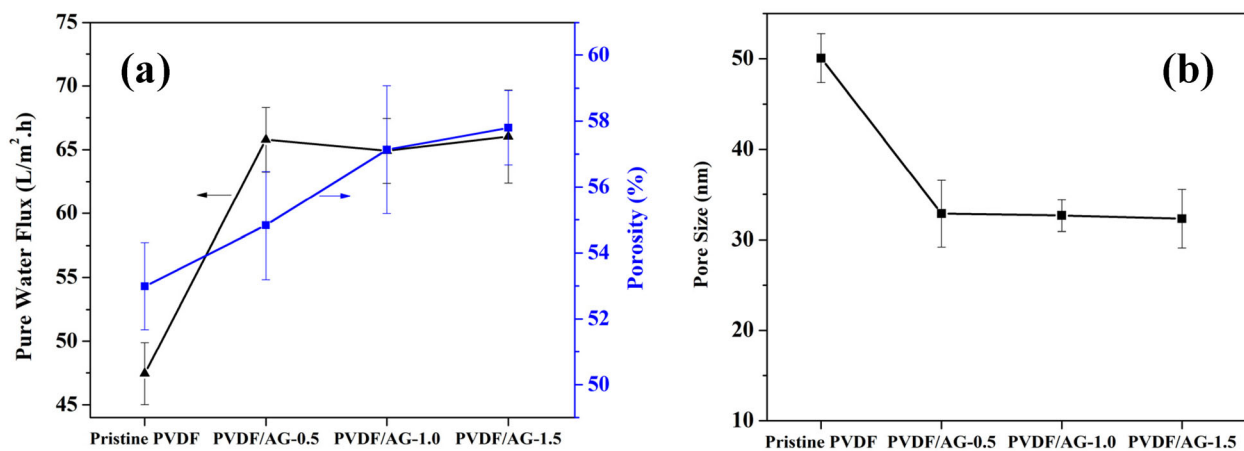
Table 2. The elemental composition of Gum Arabic.

		GA	
Elemental	EDX recorded	Mass (%)	Atomic (%)
Oxygen	O K	47.84	41.38
Carbon	C K	50.28	57.93
Sodium	Na K	0.52	0.31
Potassium	K K	0.14	0.05
Calcium	Ca K	0.52	0.18
Cupper	Cu K	0.70	0.15

Figure 2. Pure water flux and porosity (a); Membrane pore size (b) of all prepared membranes. The adsorptive membrane fouling was carried out at 4 bars for 60 min filtration at ambient temperature.

Table 3. Physical characteristics of membranes.

Variable	Flux (L/m^2 h)^s	Porosity (%)^{ns}	Pore size (nm)^s	Static water contact angle (^{o})^s
PVDF	47.46 ± 7.15^a	52.99 ± 0.95	50.89 ± 2.15^a	80.98 ± 0.40^a
PVDF/AG-0.5	65.79 ± 0.28^b	54.83 ± 0.74	32.89 ± 3.18^b	75,61 ± 1.00^b
PVDF/AG-1.0	64.92 ± 3.31^b	57.13 ± 1.13	31.60 ± 2.58^b	72,33 ± 0.29^c
PVDF/AG-1.5	66.04 ± 3.53^b	57.80 ± 5.90	32.38 ± 2.23^b	71,08 ± 1.00^c

The lowercase letter s represents significant differences ($p \leq 0.05$) for samples at the same parameters. The alphabets lowercase letter mean grouping on that parameters: a, group 1; b, group 2; and c, group 3. The lowercase letter in each column with the same letters are not significantly different at $p < 0.05$.
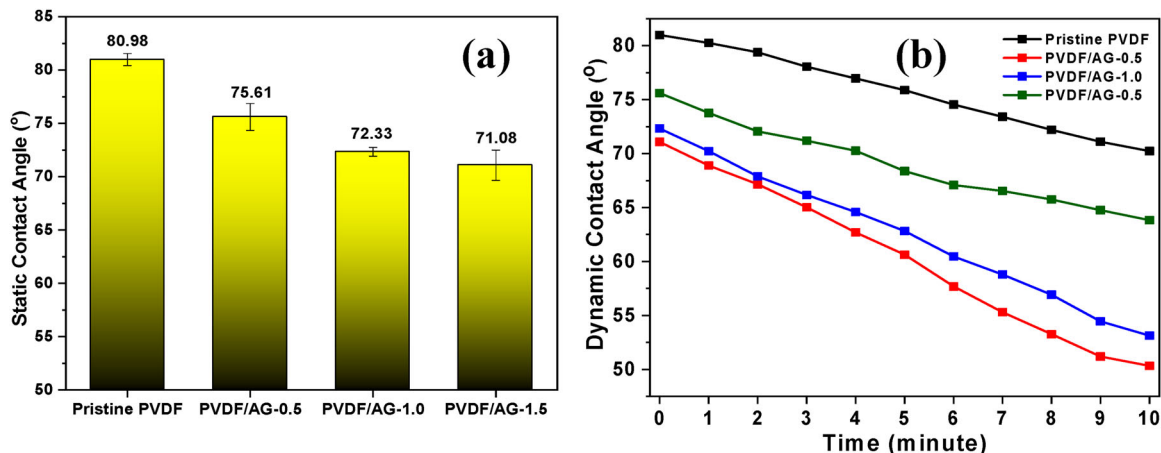
Figure 3. The static (a) and dynamic (b) water contact angles of all prepared membrane.

stream.[8,32–34] Different results were obtained in this research. Although there is an increase in porosity value, which correlates with an increase in flux value, Table 3 demonstrates no significant difference between porosity and flux values. In contrast, there is a considerable difference between porosity and flux values. Consequently, porosity is not the primary factor in the variation in flux value. Table 3 also shows that the difference in flux value is due to the static contact angle value. This statement is also supported by the same results in research conducted by Moradi et al.[35] and Mokarizadeh and Raisi.[36]

Meanwhile, the average pore size of the prepared membrane calculated was between 31 and 50 nm, as seen in Figure 2b. The interaction among PVDF (polymer), DMAc (solvent), and AG (nonsolvent) increases the thermodynamic instability in the dope solution. In principle, the rapid exchange between solvent and nonsolvent when a cast membrane was immersed in the coagulation bath resulted in a highly porous membrane structure.[37] However, adding AG into PVDF dope solution decreased membrane pore size. This could be because the effect of AG may increase the viscosity of the casting solution, contributing to a decrease in the de-mixing process during nonsolvent-induced phase separation (NIPS), leading to smaller membrane pores.[38]

3.3. Membrane hydrophilicity

Wettability is a key factor influencing the fouling resistance of membranes. The static water contact angle (SWCA) and dynamic water contact angle (DWCA) of the prepared membranes is depicted in Figure 3. Figure 3a illustrates the value of SWCA, which explains that there is a decrease in the WCA value on the modified PVDF membrane. The

addition of GA increased the hydrophilicity of the membrane. The pristine PVDF membrane showed the highest SWCA of $80.98 \pm 0.56°$, indicating the least hydrophilicity due to the hydrophobic behavior of the PVDF polymer. The GA incorporation reduced the SWCA to $75.61 \pm 1.41°$; $72.33 \pm 0.41°$, and $71.08 \pm 1.25°$ for PVDF/AG-0.5, PVDF/AG-1, and PVDF/AG-1.5, respectively. This contact angle value is related to the membrane PWF value which shows the opposite correlation. The greater the PWF value, the smaller the WCA value. This happens because the surface of the membrane is in contact with water, occurs interactions on the membrane surface. The greater the adhesion force between the membrane surface and the water, the greater the WCA value. The reduction in WCA value indicates the higher hydrophilicity of a membrane.[39,40]

Figure 3b shows the DWCA values on the membrane. The result showed that on the first drop at 0 s, the PVDF/AG-1.5 had the lowest WCA among all prepared membranes. Further, throughout at 600 s, the addition of AG may contribute to decreased WCA of PVDF membrane, resulting in improved hydrophilicity of AG incorporated PVDF membrane. For instance, the difference WCA from 0 s up to 600 s was $10.75°$, $11.78°$, $19.18°$, and $20.74°$ for pristine PVDF membrane, PVDF/AG-0.5, PVDF/AG-1, and PVDF/AG-1.5, respectively. The higher gap of WCA at 0 s and 600 s signifies the higher hydrophilicity of the membrane. PVDF/AG-1.5 had the best hydrophilicity among all membranes with a lower WCA of $50.34°$ at 600 s. This result might be ascribed to the hydroxyl functional group of AG contributing to enhancing the hydrophilicity of the membrane's surface.[41,42] The data of flux value agreed to this outcome result. Enhancement of hydrophilicity could improve membrane performance, especially in flux of membrane.
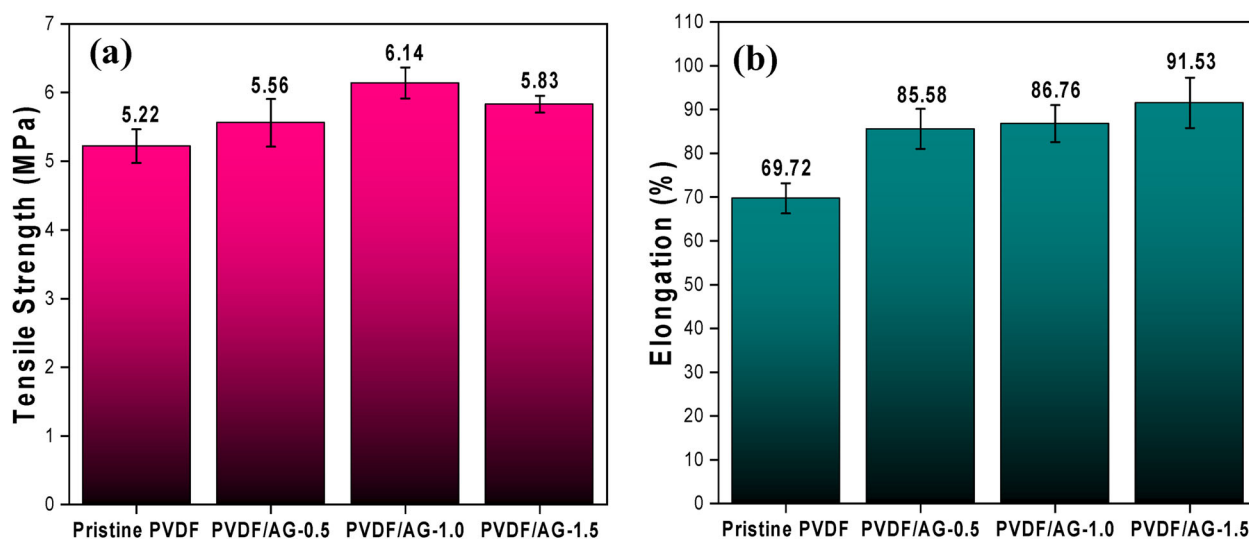
Figure 4. Mechanical test on membrane: tensile strength (a) and elongation (b).

3.4. Mechanical studies

The mechanical observation helps predict the membranes' durability and pressure capability. The result of tensile strength and percentage elongation of the membranes was demonstrated in Figure 4. The addition of AG into PVDF membrane solution influenced the mechanical property of membranes. The pristine PVDF membrane obtained the lowest tensile strength. Compared to pristine PVDF membrane, incorporating AG 0.5 wt% and 1 wt% improve tensile strength to 5.56 MPa and 6.14 MPa. However, further increasing AG concentration to 1.5 wt% reduces tensile strength to 5.83 MPa. The slight decrease of tensile strength for PVDF/AG-1.5 could enhance membrane porosity. The membrane with a highly porous structure demonstrated lower mechanical properties, similar to another study.[43] There is a tradeoff between a membrane's tensile strength and porosity. In other words, the membrane's tensile strength may decrease slightly as its porosity increases. Hassankiadeh et al.[44] utilized a variety of pore-forming additives to enhance the permeability of TIPS-prepared PVDF/PolarClean hollow fiber membranes. The membranes' porosity and permeability increased by nearly a factor of a thousand. However, the membranes' tensile strength decreased from 6 to 1 MPa, illustrating this tradeoff. However, the reduction in tensile strength was negligible enough for practical applications. In another instance, Rajabzadeh et al.[45] devised PVDF hollow fiber membrane to understand membrane properties in their study. They discovered that with the addition of PVP, both porosity and water permeability decreased. In contrast, the PVP additive substantially increased the membranes' mechanical strength, particularly their tensile strength (2–7 MPa). Under practical operating conditions, the decrease in tensile strength did not substantially affect the membrane's stability and performance. The tradeoff between membrane porosity and tensile strength is a common occurrence. However, the degree of compromise depends on the specific application and membrane performance requirements.

Likewise, as observed in Figure 4b, adding AG to PVDF membrane dope solution has increased the elongation of membranes. Pristine PVDF membrane had an elongation value of 68.5% only. Compared to other polymer materials usually used to manufacture membranes, this is quite good. For example, PES membranes have an elongation of 7.89%[46] and PVC with elongation value of 14.2%.[29] This mechanical resistance is one of the advantages of PVDF material. The modified membrane, added with AG, showed an increase in elongation yield from 0.5% to 1.5%. The highest value was recorded on the PVDF/AG-1.5 membrane, with a value of 94.2%.

This increase can be attributed to its plasticity effect and the non-polar phase (hydrophobic side) of the Arabic gum that interacts with the α and ε polymorphs in hydrophobic bonds of the PVDF, which serves as a bridge to strengthen the porous structure of the membrane.[21,47] Adding more AG in the membrane can create a plasticizing effect, increasing mechanical strength. Therefore, incorporating AG improves not only the rejection parameters but also the mechanical characteristics that can benefit the mechanical resistance and stress of the membrane.

3.5. FTIR result

The surface chemistry structures of pristine and modified membranes were analyzed by FTIR, as shown in Figure 5.

The presence of a peak at 3024 cm^{-1} signed to the C–H ring stretching vibration in PVDF membrane.[48,49] The FTIR of PVDF membrane commonly appeared in some wavenumbers, such as at 1172 cm^{-1} and 1424 cm^{-1}, attributed to the symmetrical stretching of –CF$_2$ and C–C groups.[50] Further, the peak at 1664 cm^{-1} is assigned to the C=C adsorption of PVDF.[51,52] In the AG spectrum, three significant peaks appeared at 600 cm^{-1} was attributed to the stretching of pyranose in polysaccharides, the peak at 1050 cm^{-1} implied the presence of –CH band in polysaccharides, and the peak at 3000–3500 cm^{-1} for amino groups, which undercover by the absorption peak at 3200 cm^{-1} for –OH groups. Compared to the pristine PVDF membrane, the PVDF/AG-1 and PVDF/AG-1.5 showed a new peak at 3234 cm^{-1}, 957 cm^{-1}, and 610 cm^{-1}, which can be assigned to the presence of –OH groups, –CH band, and pyranose of AG on the membrane surface.
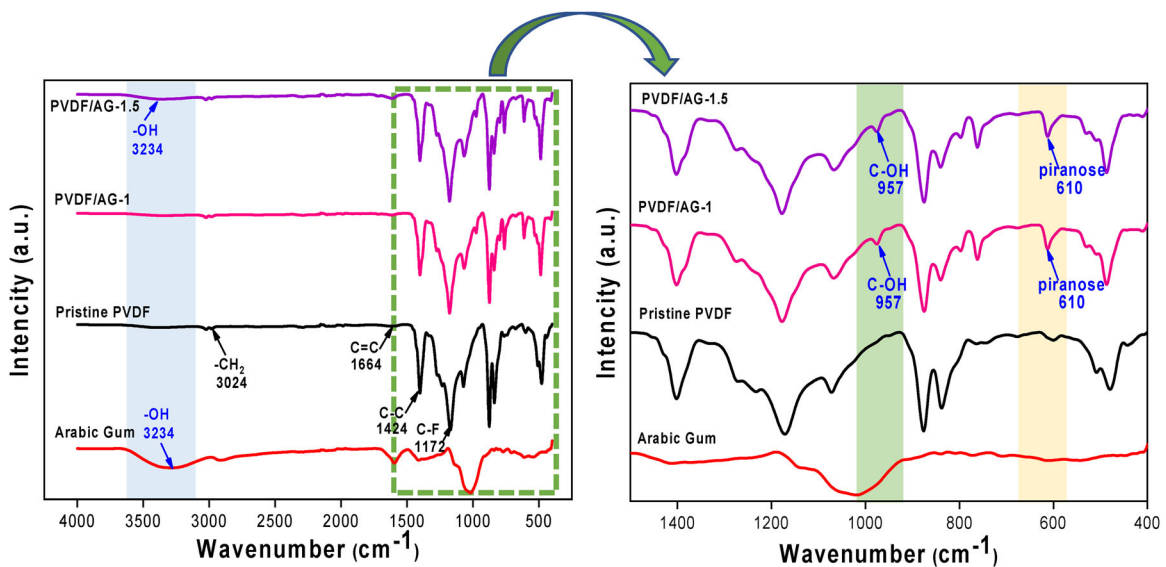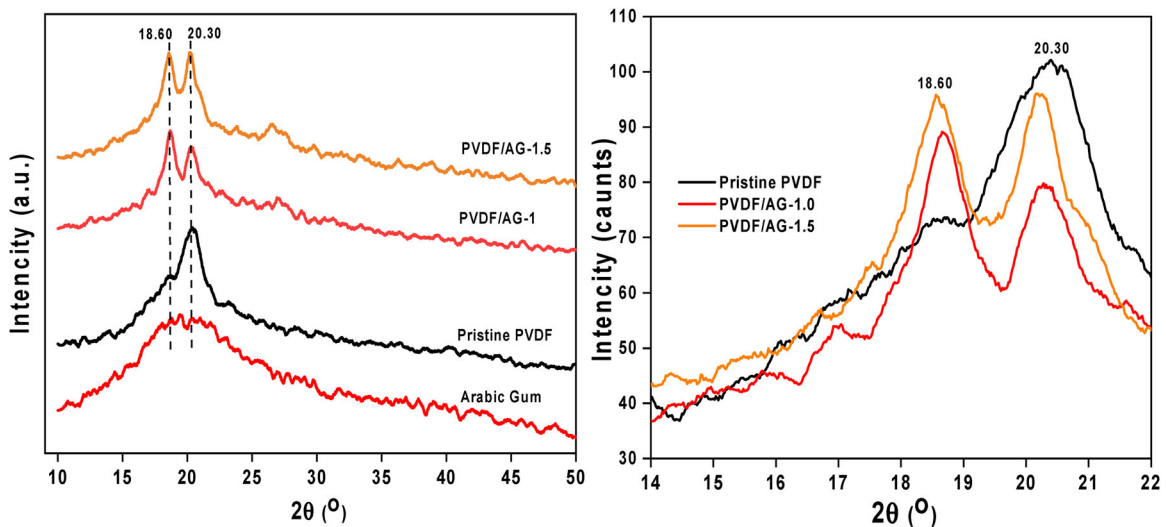
Figure 5. FTIR spectra of PVDF/AG membranes.

Figure 6. XRD diffractograms of PVDF/AG membrane.

Table 4. The integral result of XRD data of PVDF membrane.

Membrane	Center	FWHM	Height	Area
Pristine PVDF	18.64°	3.897	65.931	218.171
	20.32°	4.621	94.435	381.681
PVDF/AG-1.0	18.66°	3.007	81.865	251.352
	20.28°	5.241	72.501	259.307
PVDF/AG-1.5	18.56°	3.092	87.865	278.240
	20.26°	3.123	88.117	298.235

3.6. XRD result

Figure 6 exhibits the XRD pattern of the AG-incorporated PVDF membrane. The result demonstrated that the diffraction peak at 18.60° and 20.30° reveals the characteristic crystal structure of ɤ and ß in pure PVDF membrane.[53] The peak area on each XRD graph was calculated using the peaks and baseline with the integrated peaks method in the Originpro software. The data for peak area results are shown in Table 4. The PVDF graph has an area of 218,171 with a peak height of 65,931 at peak 18.64° and an area of 381,681 with a peak height of 94,435 at peak 20.32°. Figure 6 also shows that the

PVDF membrane has an amorphous character. while the structure of Arabic gum also shows an amorphous form with a peak of 18.60° to 20.80°. The similarity of the crystal structure between PVDF and AG causes better mixing between PVDF and AG polymers and good molecular interactions.

The addition of AG to the PVDF membrane showed a decrease in area at the peak of 20.30°. On the PVDF/AG-1.0 membrane, the peak area decreased to 259,307 and the peak height became 72,501, while on the PVDF/AG-1.5 membrane, the area decreased to 298,235 with a peak height of 88,117, at a peak of 18.60° there was a significant increase in the PVDF/AG-1.5 membrane up to 278.240 with a peak height of 87,865. Increasing the concentration of AG in the membrane increases the intensity of the 18.60 peaks which is getting higher, so that the molecular interactions between PVDF and AG mix well, indicate the formation of amorphous crystalline structure in PVDF/AG-1.5 membrane structure. On the other hand, the sharpness peak at 20.60° clearly decreased after incorporating AG to PVDF membrane, resulting in a decrease
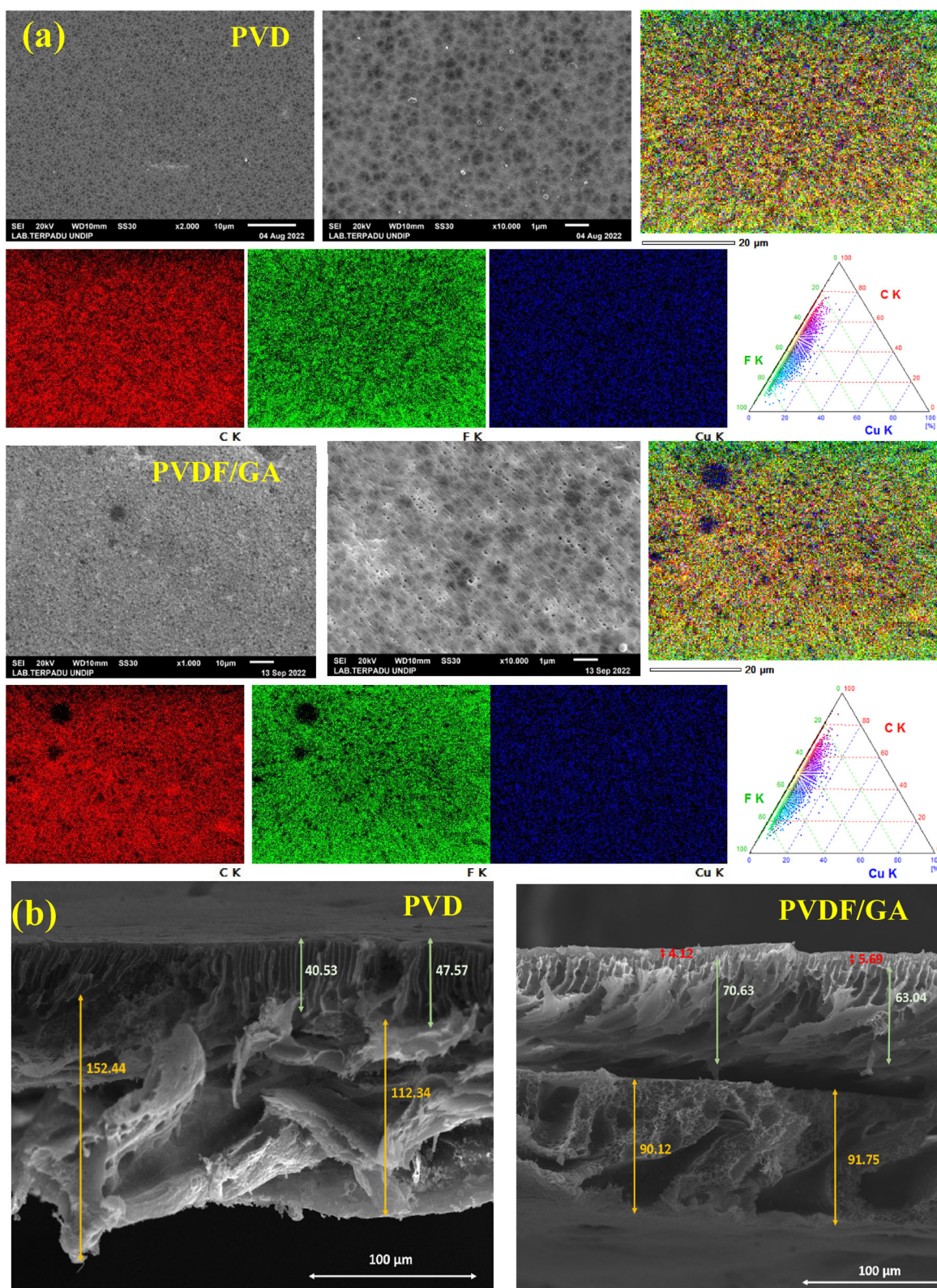
Figure 7. SEM image of membrane: morphology surface and EDX mapping and overlay plot of elemental distribution (a) and cross section morphology of PVDF membrane (b).

in the crystallinity of PVDF/AG-1.5 membrane. Hence, adding AG incorporating PVDF membrane improves intermolecular interaction between additives and polymers.[54] Thus, the PVDF/AG-1.5 membrane has the good intermixed ability and strong chemical interaction.

3.7. Surface morphology of membranes

Figure 7 demonstrates SEM images of pristine PVDF and modified membranes PVDF. Figure 7b shows the cross-section SEM–EDX images of pristine PVDF and PVDF/AG1.5 membrane. The prepared PVDF membrane depicted an

Table 5. The elemental composition of pristine PVDF and PVDF/AG-1.5 membrane.

Elemental	EDX recorded	Pristine PVDF Mass (%)	Pristine PVDF Atomic (%)	PVDF/AG-1.5 Mass (%)	PVDF/AG-1.5 Atomic (%)
Fluorine	F K	52.86	41.74	52.04	40.95
Carbon	C K	46.54	58.18	47.34	58.90
Cupper	Cu K	0.60	0.14	0.62	0.15

asymmetric structure, indicating a dense selective top layer and a support layer with finger shaped pores. The PVDF/AG-1.5 membrane showed larger finger-shaped pores than the pristine PVDF membrane.

Furthermore, it was observed that the pristine PVDF and PVDF/AG-1.5 membrane has a fingerlike structure ($43.26 \pm 2.57\,\mu m$ and $66.83 \pm 4.87\,\mu m$) and macropore layer ($132.46 \pm 4.29\,\mu m$ and $90.14 \pm 1.12\,\mu m$), respectively. Meanwhile, the new layer was found on the active surface in PVDF/AG-1.5 membrane with a thickness of $4.90 \pm 0.38\,\mu m$. The formation of a new active layer on PVDF/AG-1.5 membrane surface provided the membrane has more particular properties than the pristine PVDF membrane. It could be due to the AG additive increasing membrane surface pore when mass transfer between solvent and nonsolvent demixing process.

Meanwhile, the pristine PVDF and PVDF/AG-1.5 membrane's surface SEM images were displayed in Figure 7a. It is demonstrated that adding AG incorporated to PVDF membrane increases pore formation on membrane surface. This could be ascribed to AG's hydrophilic property, which enhances membrane hydrophilicity. The pristine PVDF and PVDF/AG-1.5 membrane contained three elements: C, F, and Cu. The elemental composition data on PVDF and PVDF/AgG-1.5 membranes are shown in Table 5. Compared to the pristine PVDF membrane, adding AG incorporated PVDF membrane clearly increases the number of C and Cu elements from 46.54% to 47.34% and 0.6% to 0.62%, respectively. On the other hand, the PVDF/AgG-1.5 membrane successfully increased elements of C and Cu by 0.8% and 0.02%, respectively. Moreover, the elements are evenly distributed over the entire membrane surface, as shown in Figure 7a.

3.8 Antifouling performance test

The experiment was conducted using BSA as a biological foulant to evaluate the separation performance of the membranes. The rejection result for BSA foulants was plotted in Figure 8a. The result demonstrated that all modified PVDF membranes successfully rejected over 80% of BSA. Compared to all modified PVDF membranes, the pristine PVDF membrane has a rejection ability of 58% BSA. This indicates that the increase in surface porosity of the membrane had not to affect for BSA rejection efficiency.

Meanwhile, Figure 8c shows the antifouling properties of membranes for filtration time (up to 90 min) using a feed solution containing BSA concentration (1000 mg/L). The result revealed that all modified membranes demonstrated higher flux than the pristine PVDF membrane, indicating that modified membranes have better antifouling properties. However, all membranes showed a similar trend (the fluxes

dropped rapidly in the first few minutes, followed by a stable flux decline at the end of filtration). This phenomenon could be due to the concentration polarization on membrane surface, increasing protein deposition on the membrane surface. Similar result to Figure 8d, the effects of protein deposition on membrane surface also contribute to reducing normalized flux (J/J_o) of membranes. Indeed, the addition of 1.5 wt%, 1 wt%, and 0.5 wt% of AG increased the normalized flux of $\sim75\%$, $\sim57\%$, and $\sim61\%$, respectively. Compared to modified membranes, the pristine PVDF membrane had a normalized flux $\sim37\%$.

On the other hand, the extent of flux recovery (FR) after BSA fouling was analyzed using the FR index, and the results are shown in Figure 8b. Unsurprisingly, the pristine PVDF and PVDF/AG-1.5 membranes demonstrated the lowest and highest FR of 32% and 74%, respectively. Meanwhile, the reduction of flux recovery when the result of rejection and flux of membrane followed the addition of AG from 0.5 wt% to 1.0 wt%. Even though the rejection and flux of PVDF/AG-0.5 membrane were slightly higher than PVDF/AG-1.0, PVDF/AG-1.0 obtained better membrane performance than PVDF/AG-0.5 membrane. It confirms that the addition of AG has successfully enhanced membrane hydrophilicity. A high hydrophilicity is assumed to decrease the hydrophobic interaction between BSA molecules and the membrane structure.

Generally, the increased normalized flux could improve membrane fouling resistance, as shown in Figure 8e. The outcome of resistance is divided into R_m, R_c, R_f, and R_t. In this study, the better membrane performance showed a lesser fouling resistance value. The result showed the lowest among all prepared membranes, the R_m, R_c, R_f, and R_t of PVDF/AG-1.5 membranes. These results indicated that incorporating AG into PVDF membranes could promote PVDF membranes with better antifouling performance. The reversible (F_r), irreversible (Fi_r), and total (F_t) fouling ratios were three essential parameters for investigating the antifouling property of the prepared membranes. The F_r, Fi_r, and F_t parameters are presented in Figure 8f. It showed that the percentage of Fi_r and F_t of PVDF/AG-1.5 membrane was lowest compared to other modified membranes, while the weakest of F_r was obtained by PVDF/AG-0.5 membrane. The reversible fouling in membrane filtration (F_r) can be removed by mechanical or chemical membrane washing.[55] Thus, the result is consistent with water contact angle results. In principle, enhancing hydrophilicity on the membrane surface could increase the wettability and reduce irreversible fouling ratio.

3.9. Membrane stability test

The membranes with the best AG, namely PVDF/AG-1.5 membranes, were tested for stability. The membrane was tested for stability by immersing it in distilled water for 14 days and shaking it at 100 rpm. FTIR then tested the membrane to determine the groups of AG contained in this membrane. Figure 9 depicts the results of the FTIR test. The AG functional groups were still present in the soaked PVDF/AG-1.5 membrane at the peak of $610\,cm^{-1}$ for the pyranose
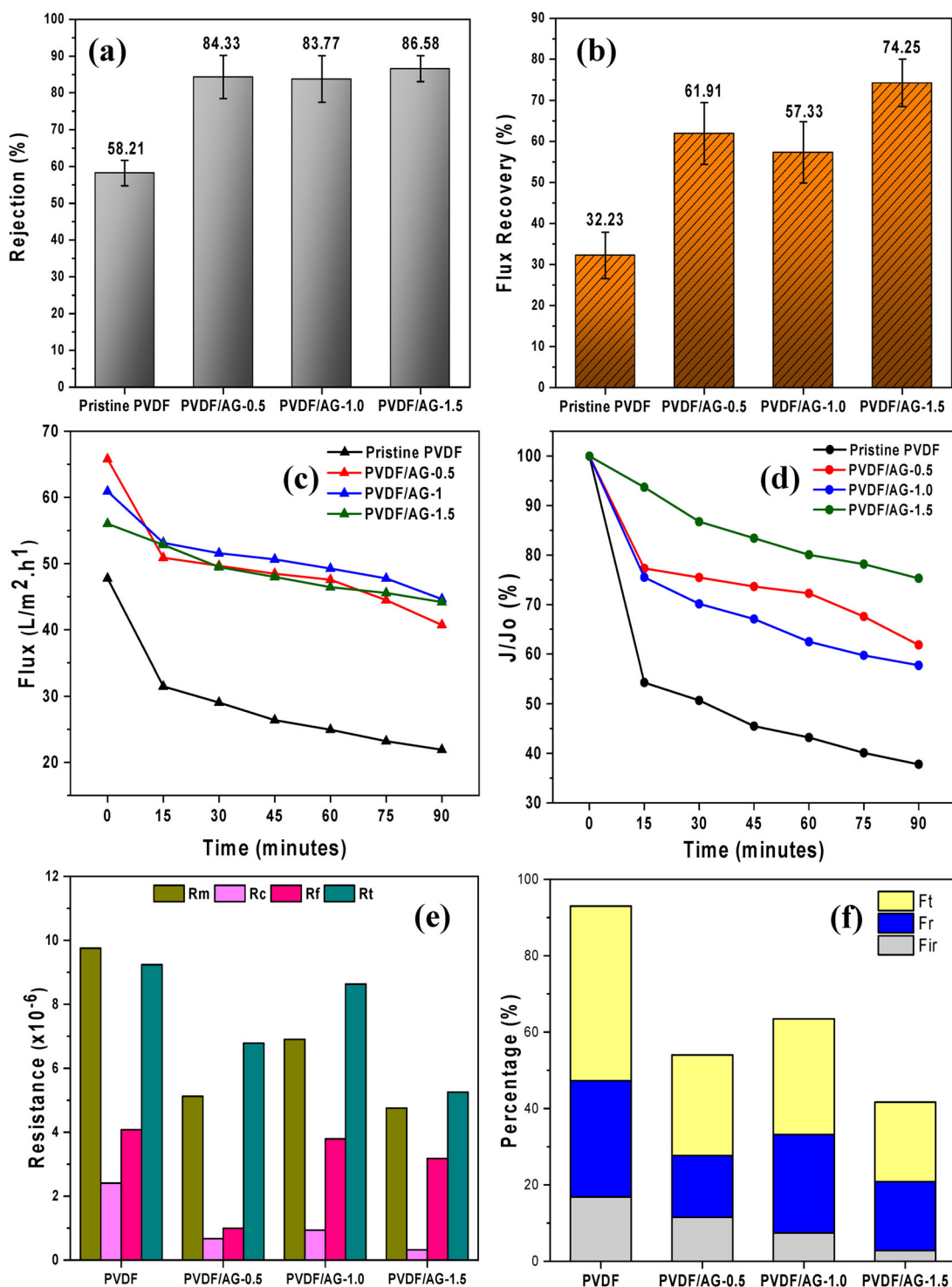
Figure 8. Antifouling performance: BSA rejection (a); flux recovery (b); actual permeate fluxes of BSA filtration (c); normalized BSA wastewater filtration (d); fouling ratio (e) and fouling resistance (f).

group, 957 cm^{-1} for the C–OH group, and 3234 cm^{-1} for the –OH group. This group shows that there is no significant reduction in transmittance value. This indicates that the AG compound is well retained in the membrane matrix. When AG is immersed in distilled water for an extended period of time, it does not leach. A cross-flow test with several filtration cycles was performed to better understand the membrane's performance with the addition of AG.

Cross-flow filtration was used to test the membrane's performance over four cycles. After each cycle, the membrane

is washed with distilled water and tested for filtration with BSA foulant solution. The performance of the membranes was evaluated using pristine PVDF and PVDF/AG-1.5 membranes. Figure 10 depicts the results of the cross-flow test. In the first cycle filtration test, the PVDF pristine membrane had an initial flux of 49.82 L m^{-2} h^{-1}; after 90 min of testing with BSA solution, the flux decreased to 35.24 L m^{-2} h^{-1}. After washing with distilled water, the flux increases. The decline, however, continued until the BSA permeate flux was only 16.17 L m^{-2} h^{-1} in cycle 4. The flux in the first
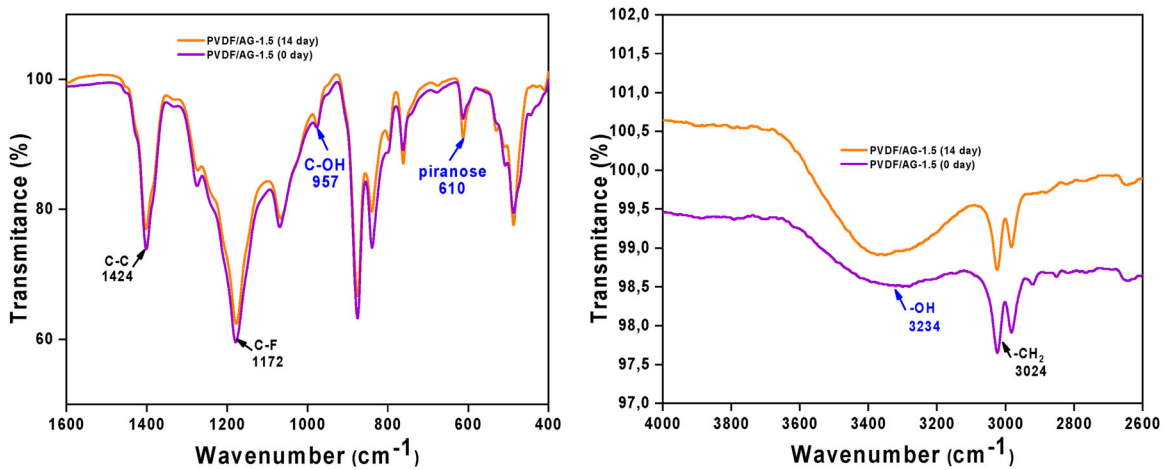
Figure 9. FTIR spectra of PVDF/AG membranes after the stability test.
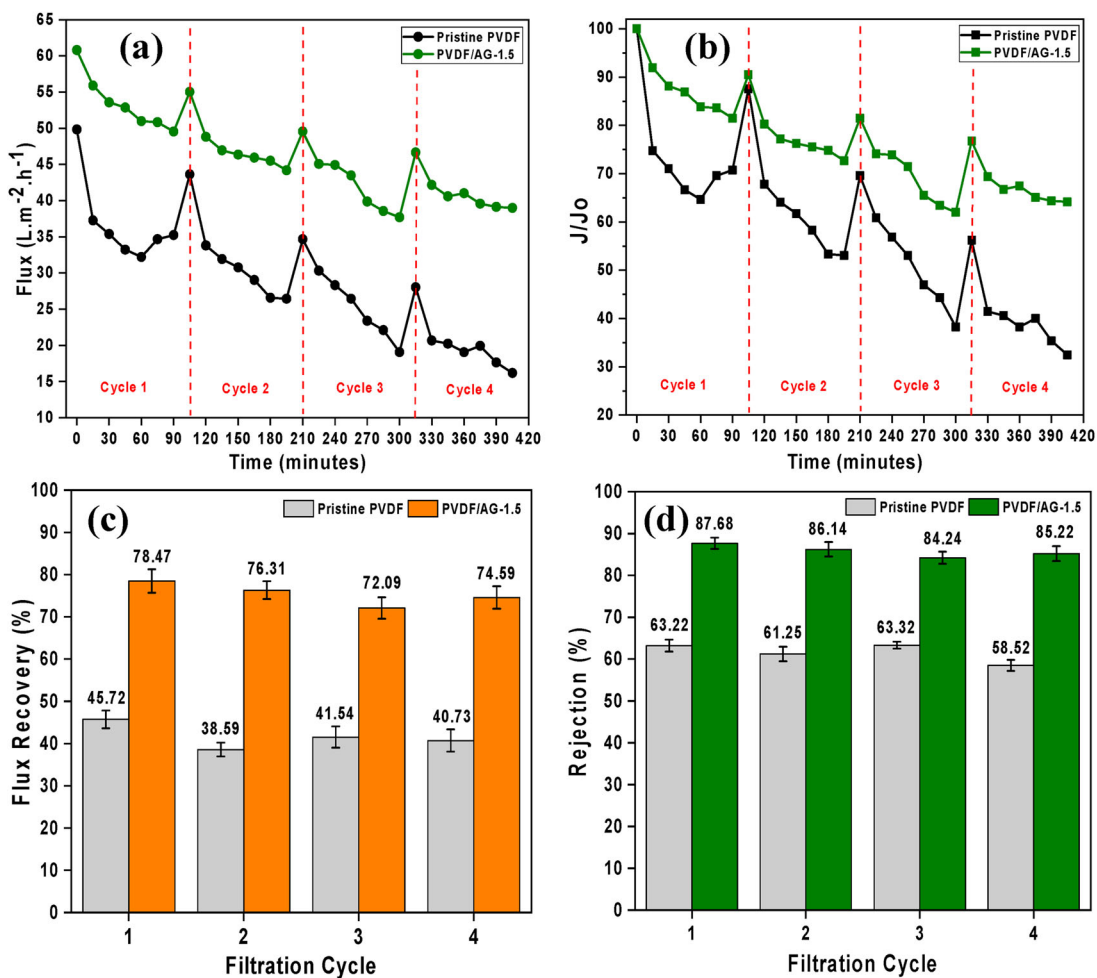
Figure 10. Membrane's recycle performance of pristine PVDF and PVDF/AG-1.5: Actual permeate fluxes of BSA filtration (a); normalized BSA wastewater filtration (b); flux recovery (c) and BSA rejection (d).

cycle was $60.80\,\text{L m}^{-2}\,\text{h}^{-1}$ on the PVDF/AG-1.5 membrane. The flux dropped to $49.53\,\text{L m}^{-2}\,\text{h}^{-1}$ in the first 90 min. After washing in cycle 2, the flux increased to $55.02\,\text{L m}^{-2}\,\text{h}^{-1}$. Until the fourth cycle, the flux is reduced to $38.99\,\text{L m}^{-2}\,\text{h}^{-1}$.

Figure 10b shows that the normalized flux J/J_o values of the pristine PVDF and PVDF/AG-1.5 membranes have decreased. However, the decrease in pristine PVDF membranes was more significant. The PVDF pristine membrane's J/J_o value was 70.75% in the first cycle, while the PVDF/AG-1.5 value was 81.47%. The J/J_o values of each membrane increased after washing with distilled water to 87.53% and 90.49% for pristine PVDF and PVDF/AG-1.5 membranes, respectively. In cycle 4, the J/J_o value continued to fall until the remaining pristine PVDF membrane had a value of 32.46%, and the PVDF/AG-1.5 membrane had a

Table 6. Comparison of filtration and antifouling performance of modified membranes from other studies and this study.

Membrane code	Pure water flux (L/m² h)	Foulant rejection (%)	Flux recovery (%)	Contact angle (°)	Ref.
PVDF/MWCNT/Chl-Ag	158.55 at 4 bar	99.99 for turbidity removal	97.24	46.59	[56]
PVDF/ZnO@ZIF	395 at 10 bar	80.10 for BSA removal	94	–	[57]
PVDF/PHMG/TA	1734 at 10 bar	99% for tween removal	96.24	38	[55]
PVDF/PLA	376.7 at 1.5 bar	97 for HA removal	–	~70	[43]
PVDF/PPy/ox-MWCNT	399 at 2 bar	98 for BSA removal	59.8	67.50	[58]
PVDF/HFSN	559.8 at 1 bar	96.6 for BSA removal 97.7 for HA removal	–	–	[1]
PVDF/AG	**66.04 at 3 bar**	**86.58 for BSA removal**	**74.25**	**71.08**	**This study**

value of 64.13%. The PVDF/AG-1.5 membrane's J/J_o value being more significant than the pristine PVDF membrane indicates that the PVDF/AG-1.5 membrane's performance value is better than the pristine PVDF membrane. Modification with AG increases the ability of the PVDF membrane against BSA foulants. The normalized flux (J/J_o) value of the PVDF/AG-1.5 membrane increased 2 times compared to the pristine PVDF membrane.

This is also consistent with the flux recovery value shown in Figure 10c flux recovery values for PVDF pristine membranes are in the range of 38–46%. at the same time, the PVDF/AG-1.5 membrane is in the range of 72–78%. PVDF/AG-1.5 membranes have nearly twice the flux recovery ability of pristine PVDF membranes. The filtration performed up to four times in this cycle revealed that the flux recovery value on the PVDF/AG-1.5 membrane remained stable. As a result, the PVDF/AG-1.5 membrane's performance remains excellent, and the AG compound in the membrane matrix remains stable. Figure 10 depicts the membrane's rejection value (d). It can be seen that, in addition to producing a good flux recovery value, the PVDF/AG-1.5 membrane also has a good rejection value to BSA foulant. Compared to the pristine PVDF membrane, which has a rejection value of around 60%.

3.10. Comparison with other studies

Table 6 illustrates the modified membrane's filtration and antifouling performance in previous published studies and this study. It is rather challenging to obtain an accurate investigation due to various studies' complexity of modification components. However, our AG-incorporated PVDF membranes are quite competitive with other studies.

4. Conclusion

The addition of Arabic gum into PVDF membrane via phase inversion was successfully incorporated, as indicated by FTIR, XRD, and SEM-EDX analysis. The PVDF/AG-1.5 membrane of the pure water flux from 47.46 L/m² h to 66.04 L/m² h, the hydrophilicity improvement as seen in the reduction of contact angle measurement from 80.98° to 75.61°, improved porosity from 52.99% to 57.8%. Due to the presence of oxygen functional groups from AG may probably enhance the membrane hydrophilicity, the performance in terms of flux and flux recovery for PVDF/AG-1.5 membrane was significantly improved. However, adding AG from 0.5 wt% to 1.5 wt% did not increase membrane mechanical strength and the efficiency of the membranes for BSA

rejection. Meanwhile, parameters such as R_m, R_c, R_f, R_t, Fi$_r$, and F_t of PVDF/AG-1.5 membrane were lowest compared to other modified membranes, while the lowest of F_r was obtained by PVDF/AG-0.5 membrane. The modified PVDF membranes demonstrated better antifouling membrane performance than the pristine PVDF membrane. Thus, the study shows that AG is a promising additive for preparing UF membranes with enhanced membrane performance for water treatment applications.

Disclosure statement

No potential conflict of interest was reported by the author(s).

ORCID

Radenrara Dewi Artanti Putri 🔾 http://orcid.org/0000-0002-8990-3091
Herlambang Abriyanto 🔾 http://orcid.org/0000-0003-4760-4082
Ria Desiriani 🔾 http://orcid.org/0000-0001-6940-1767
Abdullah Malik Islam Filardli 🔾 http://orcid.org/0000-0003-2490-6782
Zuhriyan Ash Shiddieqy Bahlawan 🔾 http://orcid.org/0000-0003-3872-4402
Maharani Kusumaningrum 🔾 http://orcid.org/0000-0002-3879-6644
Randi Aswar 🔾 http://orcid.org/0000-0003-3687-9275

References

[1] Wang, H.; Wang, Z. M.; Yan, X.; Chen, J.; Lang, W. Z.; Guo, Y. J. Novel Organic-Inorganic Hybrid Polyvinylidene Fluoride Ultrafiltration Membranes with Antifouling and Antibacterial Properties by Embedding N-Halamine Functionalized Silica Nanospheres. *J. Indus. Eng. Chem.* **2017**, *52*, 295–304. DOI: 10.1016/j.jiec.2017.03.059.

[2] Desiriani, R.; Susanto, H.; Aryanti, N. Performance Evaluation of Nanofiltration Membranes for Dye Removal of Synthetic Hand-Drawn Batik Industry Wastewater. *Environ. Prot. Eng.* **2022**, *48*, 51–68. DOI: 10.37190/epe220104.

[3] Desiriani, R.; Kresnowati, M. T. A. P.; Wenten, I. G. Membrane-Based Downstream Processing of Microbial Xylitol Production. *Int. J. Technol.* **2017**, *8*, 1393–1401. DOI: 10.14716/ijtech.v8i8.726.

[4] Sun, H.; Yang, X.; Zhang, Y.; Cheng, X.; Xu, Y.; Bai, Y.; Shao, L. Segregation-Induced *In Situ* Hydrophilic Modification of Poly (Vinylidene Fluoride) Ultrafiltration Membranes via Sticky Poly (Ethylene Glycol) Blending. *J. Membr. Sci.* **2018**, *563*, 22–30. DOI: 10.1016/j.memsci.2018.05.046.

[5] Yu, Y.; Yang, Y.; Yu, L.; Koh, K. Y.; Chen, J. P. Modification of Polyvinylidene Fluoride Membrane by Silver Nanoparticles-Graphene Oxide Hybrid Nanosheet for Effective Membrane Biofouling Mitigation. *Chemosphere* **2021**, *268*, 129187. DOI: 10.1016/j.chemosphere.2020.129187.

[6] Bai, H.; Wang, X.; Zhou, Y.; Zhang, L. Preparation and Characterization of Poly(Vinylidene Fluoride) Composite Membranes Blended with Nano-Crystalline Cellulose. *Prog. Nat. Sci.: Mater. Int.* **2012**, *22*, 250–257. DOI: 10.1016/j.pnsc.2012.04.011.

[7] Sri Abirami Saraswathi, M. S.; Rana, D.; Kaleekkal, N. J.; Divya, K.; Nagendran, A. Investigating the Efficacy of PVDF Membranes Customized with Sulfonated Graphene Oxide Nanosheets for Enhanced Permeability and Antifouling. *J. Environ. Chem. Eng.* **2020**, *8*. DOI: 10.1016/j.jece.2020.104426.

[8] Susanto, H.; Malik, A. I. F.; Raharjo, S. H.; Nur, M. Preparation and Characterization of High Flux Polypropylene Microfiltration Membrane via Non-Solvent Induced Phase Separation. *Mater. Today Proc.* **2019**, *13*, 276–280. DOI: 10.1016/j.matpr.2019.03.227.

[9] Chen, Z.; Chen, G. E.; Xie, H. Y.; Xu, Z. L.; Li, Y. J.; Wan, J. J.; Liu, L. J.; Mao, H. F. Photocatalytic Antifouling Properties of Novel PVDF Membranes Improved by Incorporation of SnO_2-GO Nanocomposite for Water Treatment. *Sep. Purif. Technol.* **2021**, *259*. DOI: 10.1016/j.seppur.2020.118184.

[10] Xu, Y.; An, L.; Chen, L.; Cao, L.; Zeng, D.; Wang, G. A Facile Chemical Route to Synthesize Zn Doped Hydroxyapatite Nanorods for Protein Drug Delivery. *Mater. Chem. Phys.* **2018**, *214*, 359–363. DOI: 10.1016/j.matchemphys.2018.04.117.

[11] Rahimpour, A.; Jahanshahi, M.; Rajaeian, B.; Rahimnejad, M. TiO_2 Entrapped Nano-Composite PVDF/SPES Membranes: Preparation, Characterization, Antifouling and Antibacterial Properties. *Desalination* **2011**, *278*, 343–353. DOI: 10.1016/j.desal.2011.05.049.

[12] Abriyanto, H.; Susanto, H.; Maharani, T.; Filardli, A. M. I.; Desiriani, R.; Aryanti, N. Synergistic Effect of Chitosan and Metal Oxide Additives on Improving the Organic and Biofouling Resistance of Polyethersulfone Ultrafiltration Membranes. *ACS Omega* **2022**. DOI: 10.1021/acsomega.2c03685.

[13] Liu, Q.; Huang, S.; Zhang, Y.; Zhao, S. Comparing the Antifouling Effects of Activated Carbon and TiO_2 in Ultrafiltration Membrane Development. *J. Colloid Interface Sci.* **2018**, *515*, 109–118. DOI: 10.1016/j.jcis.2018.01.026.

[14] Kajau, A.; Motsa, M.; Mamba, B. B.; Mahlangu, O. Leaching of CuO Nanoparticles from PES Ultrafiltration Membranes. *ACS Omega* **2021**, *6*, 31797–31809. DOI: 10.1021/acsomega.1c04431.

[15] Azhar, F. H.; Harun, Z.; Hubadillah, S. K.; Ahmad, R. A. R.; Sazali, N.; Bahri, S. S.; Ibrahim, S. A.; Hussin, R. Fabrication of Mixed Matrix Membrane Containing Chlorophyll Extracted from Spinach for Humic Acid Removal. In *Materials Today: Proceedings*; Elsevier Ltd, 2020; Vol. 46, pp 2058–2064. DOI: 10.1016/j.matpr.2021.03.200.

[16] Elizalde, C. N. B.; Al-Gharabli, S.; Kujawa, J.; Mavukkandy, M.; Hasan, S. W.; Arafat, H. A. Fabrication of Blend Polyvinylidene Fluoride/Chitosan Membranes for Enhanced Flux and Fouling Resistance. *Sep. Purif. Technol.* **2018**, *190*, 68–76. DOI: 10.1016/j.seppur.2017.08.053.

[17] Liu, C. X.; Zhang, D. R.; He, Y.; Zhao, X. S.; Bai, R. Modification of Membrane Surface for anti-Biofouling Performance: Effect of Anti-Adhesion and Anti-Bacteria Approaches. *J. Membr. Sci.* **2010**, *346*, 121–130. DOI: 10.1016/j.memsci.2009.09.028.

[18] Biao, L.; Tan, S.; Wang, Y.; Guo, X.; Fu, Y.; Xu, F.; Zu, Y.; Liu, Z. Synthesis, Characterization and Antibacterial Study on the Chitosan-Functionalized Ag Nanoparticles. *Mater. Sci. Eng. C* **2017**, *76*, 73–80. DOI: 10.1016/j.msec.2017.02.154.

[19] Ali, B. H.; Ziada, A.; Blunden, G. Biological Effects of Gum Arabic: A Review of Some Recent Research. *Food Chem. Toxicol.* **2009**, *47*, 1–8. DOI: 10.1016/j.fct.2008.07.001.

[20] Manning, H. E.; Bird, M. R. Gum Arabic Fractionation Using Synthetic Membranes: The Importance of Fouling. *Food Bioprod. Process.* **2015**, *93*, 298–303. DOI: 10.1016/j.fbp.2014.10.008.

[21] Manawi, Y.; Kochkodan, V.; Mohammad, A. W.; Ali Atieh, M. Arabic Gum as a Novel Pore-Forming and Hydrophilic Agent in Polysulfone Membranes. *J. Membr. Sci.* **2017**, *529*, 95–104. DOI: 10.1016/j.memsci.2017.02.002.

[22] Aji, M. M.; Narendren, S.; Purkait, M. K.; Katiyar, V. Biopolymer (Gum Arabic) Incorporation in Waste Polyvinylchloride Membrane for the Enhancement of Hydrophilicity and Natural Organic Matter Removal in Water. *J. Water Process Eng.* **2020**, *38*. DOI: 10.1016/j.jwpe.2020.101569.

[23] Chai, P. V.; Choy, P. Y.; Teoh, W. C.; Mahmoudi, E.; Ang, W. L. Graphene Oxide Based Mixed Matrix Membrane in the Presence of Eco-Friendly Natural Additive Gum Arabic. *J. Environ. Chem. Eng.* **2021**, *9*. DOI: 10.1016/j.jece.2021.105638.

[24] Ahmed, A. A. Health Benefits of Gum Arabic and Medical Use. In *Gum Arabic: Structure, Properties, Application and Economics*; Elsevier: Amsterdam, 2018; pp 183–210. DOI: 10.1016/B978-0-12-812002-6.00016-6.

[25] Zielińska-Przyjemska, M.; Ignatowicz, E.; Krajka-Kuźniak, V.; Baer-Dubowska, W. Effect of Tannic Acid, Resveratrol and its Derivatives, on Oxidative Damage and Apoptosis in Human Neutrophils. *Food Chem. Toxicol.* **2015**, *84*, 37–46. DOI: 10.1016/j.fct.2015.07.013.

[26] Dave, P. N.; Gor, A. Natural Polysaccharide-Based Hydrogels and Nanomaterials: Recent Trends and Their Applications. In *Handbook of Nanomaterials for Industrial Applications*; Elsevier: Amsterdam, 2018; pp 36–66. DOI: 10.1016/B978-0-12-813351-4.00003-1.

[27] Farooq, M.; Ihsan, J.; Mohamed, R. M. K.; Khan, M. A.; Rehman, T. U.; Ullah, H.; Ghani, M.; Saeed, S.; Siddiq, M. Highly Biocompatible Formulations Based on Arabic Gum Nano Composite Hydrogels: Fabrication, Characterization, and Biological Investigation. *Int. J. Biol. Macromol.* **2022**, *209*, 59–69. DOI: 10.1016/j.ijbiomac.2022.03.162.

[28] Agnihotri, A. S. M. N.; Rison, S. B. A. K.; Varghese, A. Tuning of the Surface Structure of Silver Nanoparticles Using Gum Arabic for Enhanced Electrocatalytic Oxidation of Morin. *Appl. Surf. Sci. Adv.* **2021**, *6*, 100181. DOI: 10.1016/j.apsadv.2021.100181.

[29] Moghadam, A.; Salmani Mobarakeh, M.; Safaei, M.; Kariminia, S. Synthesis and Characterization of Novel Bio-Nanocomposite of Polyvinyl Alcohol-Arabic Gum-Magnesium Oxide via Direct Blending Method. *Carbohydr. Polym.* **2021**, *260* (February), 117802. DOI: 10.1016/j.carbpol.2021.117802.

[30] Al-Ansari, M. M.; Al-Dahmash, N. D.; Ranjitsingh, A. J. A. Synthesis of Silver Nanoparticles Using Gum Arabic: Evaluation of its Inhibitory Action on *Streptococcus Mutans* Causing Dental Caries and Endocarditis. *J. Infect. Public Health* **2021**, *14*, 324–330. DOI: 10.1016/j.jiph.2020.12.016.

[31] Vuillemin, M. E.; Michaux, F.; Adam, A. A.; Linder, M.; Muniglia, L.; Jasniewski, J. Physicochemical Characterizations of Gum Arabic Modified with Oxidation Products of Ferulic Acid. *Food Hydrocoll.* **2020**, *107*. DOI: 10.1016/j.foodhyd.2020.105919.

[32] Guan, K.; Qin, W.; Liu, Y.; Yin, X.; Peng, C.; Lv, M.; Sun, Q.; Wu, J. Evolution of Porosity, Pore Size and Permeate Flux of Ceramic Membranes During Sintering Process. *J. Membr. Sci.* **2016**, *520*, 166–175. DOI: 10.1016/j.memsci.2016.07.023.

[33] Lee, W.; Kang, P. K.; Kim, A. S.; Lee, S. Impact of Surface Porosity on Water Flux and Structural Parameter in Forward Osmosis. *Desalination* **2018**, *439*, 46–57. DOI: 10.1016/j.desal.2018.03.027.

[34] Abunada, M.; Dhakal, N.; Andyar, W. Z.; Ajok, P.; Smit, H.; Ghaffour, N.; Schippers, J. C.; Kennedy, M. D. Improving MFI-UF Constant Flux to More Accurately Predict Particulate Fouling in RO Systems: Quantifying the Effect of Membrane

Surface Porosity. *J. Membr. Sci.* **2022**, 660. DOI: 10.1016/j.memsci.2022.120854.

[35] Moradi, G.; Zinadini, S.; Rajabi, L. Development of Nanofiltration PES Membranes Incorporated with Hydrophilic Para Hydroxybenzoate Alumoxane Filler for High Flux and Antifouling Property. *Chem. Eng. Res. Des.* **2020**, *158*, 148–163. DOI: 10.1016/j.cherd.2020.04.004.

[36] Mokarizadeh, H.; Raisi, A. Industrial Wastewater Treatment Using PES UF Membranes Containing Hydrophilic Additives: Experimental and Modeling of Fouling Mechanism. *Environ. Technol. Innov.* **2021**, *23*. DOI: 10.1016/j.eti.2021.101701.

[37] Montesanto, S.; Mannella, G. A.; Carfì Pavia, F.; la Carrubba, V.; Brucato, V. Coagulation Bath Composition and Desiccation Environment as Tuning Parameters to Prepare Skinless Membranes via Diffusion Induced Phase Separation. *J. Appl. Polym. Sci.* **2015**, *132*. DOI: 10.1002/app.42151.

[38] Chakrabarty, B.; Ghoshal, A. K.; Purkait, M. K. Preparation, Characterization and Performance Studies of Polysulfone Membranes Using PVP as an Additive. *J. Membr. Sci.* **2008**, *315*, 36–47. DOI: 10.1016/j.memsci.2008.02.027.

[39] Istirokhatun, T.; Rokhati, N.; Nurlaeli, D.; Arifianingsih, N. N.; Sudarno; Syafrudin; Susanto, H. Characteristics, Biofouling Properties and Filtration Performance of Cellulose/Chitosan Membranes. *J. Environ. Sci. Technol.* **2017**, *10*, 56–67. DOI: 10.3923/jest.2017.56.67.

[40] Susanto, H.; Robbani, M. H.; Istirokhatun, T.; Firmansyah, A. A.; Rhamadhan, R. N. Preparation of Low-Fouling Polyethersulfone Ultrafiltration Membranes by Incorporating High-Molecular-Weight Chitosan with the Help of a Surfactant. *S. Afr. J. Chem. Eng.* **2020**, *33*, 133–140. DOI: 10.1016/j.sajce.2020.07.003.

[41] Sinha, M. K.; Purkait, M. K. Enhancement of Hydrophilicity of Poly(Vinylidene Fluoride-Co-Hexafluoropropylene) (PVDF-HFP) Membrane Using Various Alcohols as Nonsolvent Additives. *Desalination* **2014**, *338*, 106–114. DOI: 10.1016/j.desal.2014.02.002.

[42] Wang, Y. Q.; Wang, T.; Su, Y. L.; Peng, F. B.; Wu, H.; Jiang, Z. Y. Remarkable Reduction of Irreversible Fouling and Improvement of the Permeation Properties of Poly(Ether Sulfone) Ultrafiltration Membranes by Blending with Pluronic F127. *Langmuir* **2005**, *21*, 11856–11862. DOI: 10.1021/la052052d.

[43] Aseri, N. S.; Lau, W. J.; Goh, P. S.; Hasbullah, H.; Othman, N. H.; Ismail, A. F. Preparation and Characterization of Polylactic Acid-Modified Polyvinylidene Fluoride Hollow Fiber Membranes with Enhanced Water Flux and Antifouling Resistance. *J. Water Process Eng.* **2019**, *32*. DOI: 10.1016/j.jwpe.2019.100912.

[44] Hassankiadeh, N. T.; Cui, Z.; Kim, J. H.; Shin, D. W.; Lee, S. Y.; Sanguineti, A.; Arcella, V.; Lee, Y. M.; Drioli, E. Microporous Poly(Vinylidene Fluoride) Hollow Fiber Membranes Fabricated with PolarClean as Water-Soluble Green Diluent and Additives. *J. Membr. Sci.* **2015**, *479*, 204–212. DOI: 10.1016/j.memsci.2015.01.031.

[45] Rajabzadeh, S.; Liang, C.; Ohmukai, Y.; Maruyama, T.; Matsuyama, H. Effect of Additives on the Morphology and Properties of Poly(Vinylidene Fluoride) Blend Hollow Fiber Membrane Prepared by the Thermally Induced Phase Separation Method. *J. Membr. Sci.* **2012**, *423–424*, 189–194. DOI: 10.1016/j.memsci.2012.08.013.

[46] Lusiana, R. A.; Sangkota, V. D. A.; Sasongko, N. A.; Gunawan, G.; Wijaya, A. R.; Santosa, S. J.; Siswanta, D.; Mudasir, M.; Abidin, M. N. Z.; Mansur, S.; et al. Permeability Improvement of Polyethersulfone–Polietylene Glycol (PEG–PES) Flat Sheet Type Membranes by Tripolyphosphate-Crosslinked Chitosan (TPP-CS) Coating. *Int. J. Biol. Macromol.* **2020**, *152*, 633–644. DOI: 10.1016/j.ijbiomac.2020.02.290.

[47] Wang, J.; Yi, M.; Shen, Z.; Liu, L.; Zhang, X.; Ma, S. Enhanced Thermal and Mechanical Properties of Poly (Vinylidene Fluoride) Nanocomposites Reinforced by Liquid-Exfoliated Graphene. *J. Macromol. Sci. A: Pure Appl. Chem.* **2019**, *56*, 733–740. DOI: 10.1080/10601325.2019.1607375.

[48] Boributh, S.; Chanachai, A.; Jiraratananon, R. Modification of PVDF Membrane by Chitosan Solution for Reducing Protein Fouling. *J. Membr. Sci.* **2009**, *342*, 97–104. DOI: 10.1016/j.memsci.2009.06.022.

[49] Teng, L.; Yue, C.; Zhang, G. Epoxied SiO_2 Nanoparticles and Polyethyleneimine (PEI) Coated Polyvinylidene Fluoride (PVDF) Membrane for Improved Oil Water Separation, Anti-Fouling, Dye and Heavy Metal Ions Removal Capabilities. *J. Colloid Interface Sci.* **2023**, *630*, 416–429. DOI: 10.1016/j.jcis.2022.09.148.

[50] Hassan, F.; Mushtaq, R.; Saghar, S.; Younas, U.; Pervaiz, M.; Aljuwayid, A.; Muteb; Habila, M. A.; Sillanpaa, M. Fabrication of Graphene-Oxide and Zeolite Loaded Polyvinylidene Fluoride Reverse Osmosis Membrane for Saltwater Remediation. *Chemosphere* **2022**, *307*, 136012. DOI: 10.1016/j.chemosphere.2022.136012.

[51] Li, M.; Yang, Y.; Zhu, L.; Wang, G.; Zeng, Z.; Xue, L. Anti-Fouling and Highly Permeable Thin-Film Composite Forward Osmosis Membranes Based on the Reactive Polyvinylidene Fluoride Porous Substrates. *Colloids Surf. A: Physicochem. Eng. Asp.* **2022**, *654*. DOI: 10.1016/j.colsurfa.2022.130144.

[52] Wu, L.; Liu, Y.; Hu, J.; Feng, X.; Ma, C.; Wen, C. Preparation of Polyvinylidene Fluoride Composite Ultrafiltration Membrane for Micro-Polluted Surface Water Treatment. *Chemosphere* **2021**, *284*. DOI: 10.1016/j.chemosphere.2021.131294.

[53] Bakhshizadeh, S.; Sabzehmeidani, M. M.; Ghaedi, M.; Dashtian, K.; Abbasi-Asl, H. Preparation and Characterization of Mixed Matrix Membranes Based on PVDF Blend and Hydrophilic Molecularly Imprinted MIL-101 (Cr) as Filler for Efficient Selective Removal of Dye. *J. Environ. Chem. Eng.* **2022**, *10*. DOI: 10.1016/j.jece.2022.108864.

[54] Hester, J. F.; Banerjee, P.; Mayes, A. M. Preparation of Protein-Resistant Surfaces on Poly(Vinylidene Fluoride) Membranes via Surface Segregation. *Macromolecules* **1999**, *32*, 1643–1650. DOI: 10.1021/ma980707u.

[55] Lin, Q.; Wu, L.; Hu, W.; Wan, X.; Wu, Z.; Zhang, C. Antifouling and Antimicrobial Modification of Polyvinylidene Fluoride Micropore Membrane by Plant Tannic Acid and Polyhexamethylene Guanidine. *Surf. Interfaces* **2022**, *29*. DOI: 10.1016/j.surfin.2021.101708.

[56] Asadi, A.; Gholami, F.; Nazari, S.; Dolatshah, M. Preparation of Antifouling and Antibacterial Polyvinylidene Fluoride Membrane by Incorporating Functionalized Multiwalled Carbon Nanotubes. *J. Water Process Eng.* **2022**, *49*. DOI: 10.1016/j.jwpe.2022.103042.

[57] Li, Y. J.; Chen, G. E.; Xie, H. Y.; Chen, Z.; Xu, Z. L.; Mao, H. F. Increasing the Hydrophilicity and Antifouling Properties of Polyvinylidene Fluoride Membranes by Doping Novel Nano-Hybrid ZnO@ZIF-8 Nanoparticles for 4-Nitrophenol Degradation. *Polym. Test.* **2022**, *113*. DOI: 10.1016/j.polymertesting.2022.107613.

[58] Vatanpour, V.; Ghadimi, A.; Karimi, A.; Khataee, A.; Yekavalangi, M. E. Antifouling Polyvinylidene Fluoride Ultrafiltration Membrane Fabricated from Embedding Polypyrrole Coated Multiwalled Carbon Nanotubes. *Mater. Sci. Eng. C: Mater. Biol. Appl.* **2018**, *89*, 41–51. DOI: 10.1016/j.msec.2018.03.026.